A Surface-Stress-Based Microcantilever Aptasensor

Yang Choon Lim, Abbas Z. Kouzani, *Member, IEEE*, Wei Duan, Xiujuan J. Dai, Akif Kaynak, and Douglas Mair

***Abstract*—Biosensors based on microcantilevers convert biological recognition events into measurable mechanical displacements. They offer advantages such as small size, low sample volume, label-free detection, ease of integration, high-throughput analysis, and low development cost. The design and development of a microcantilever-based aptasensor employing SU-8 polymer as the fabrication material is presented in this paper. Aptamers are employed as bioreceptor elements because they exhibit superior specificity compared to antibodies due to their small size and physicochemical stability. To immobilise thrombin DNA aptamer on the bare SU-8 surface of the aptasensor, a combined plasma mode treatment method is implemented which modifies the surface of the aptasensor. Label-free detection of thrombin molecules using the fabricated aptasensor is successfully demonstrated. The measured deflection is one order of magnitude higher than that of a silicon nitride microcantilever biosensor. The developed aptasensor also demonstrates high specificity.**

***Index Terms*—Aptasensor, label-free, microcantilever, optical, SU-8.**

I. Introduction

BIOSENSORS are widely used in point-of care diagnostics, drug screening, proteomic, and genetic analysis. The requirement to detect different molecules at increasingly low concentrations has motivated the miniaturization of biosensors to reduce sample volume.

Antibodies were previously the receptor molecules of choice until the development of aptamers [1]. Aptamers are gaining widespread acceptance due to their better binding specificity and binding affinity compared to antibodies. Aptamers are highly regarded as the emerging class of receptor molecules due to their stability, ease of production, and cost-effectiveness which leads to the development of aptasensors [2], [3].

Different types of sensing principles have been developed, and are classified into label-based and label-free approaches. The label-based approaches include optical detection such as fluorescent [4], chemiluminescent [5] and radioactive detection [6]. The labelling could alter the properties of the host molecule, and accordingly affect the binding properties [7]. Besides, the labelling is expensive and time consuming. Therefore, the label-free approach is more suitable for the point-of-care diagnostics applications. Accordingly, the label-free approach is employed in this work.

The label-free approach consists of surface plasmon resonance [8], electrochemical [9], impedance [10], field-effect transistor [11], [12], and micromechanical detection methods. Microcantilever-based sensors have been garnering a lot of interest due to their superior sensitivity and ease of fabrication compared to other sensing methods [13]. The microcantilever-based biosensor is a label-free biosensing approach that translates the biomolecular recognition event into mechanical signals. The generated mechanical signals are dependent on the operation mode of the microcantilever. The static operation mode [14], [15] produces absolute deflection of the microcantilever beam while the dynamic operation mode produces a change in the resonance frequency upon recognition of the target molecules [16]. In a liquid environment, the static mode microcantilevers are more sensitive compared to the dynamic mode microcantilevers. This is because the dynamic mode microcantilevers suffer from a damping effect that reduces their quality factor and hence their sensitivity. Therefore, the static operation mode is employed in this work.

A read-out system is required to convert the mechanical displacement into measurable electrical signals in the static mode microcantilevers. There are various read-out methods reported in the literature including piezoresistive [17], capacitive [18], MOSFET [19], and optical [20]–[22]. Each of these methods has its own advantages and disadvantages. The piezoresistive read-out method has the advantage of ease of integration with electronic circuitry but suffers from poor sensitivity, nonlinearity in piezo response, and thermal drift. The capacitive read-out method has high sensitivity and simple electronic circuitry, and is capable of absolute displacement measurement but suffers from the interference problems such as variation of the dielectric constant in different mediums. The optical read-out method such as optical lever has high resolution and linear response, is simple, and produces absolute displacement measurement. These advantages are the motivating factors for selecting the optical read-out method in this work. However, the heat from the laser could cause the microcantilever beam to deflect, producing false positive deflection. To eliminate the error generated, a reference microcantilever is employed.

In addition, the optical read-out method can be integrated into the detection system through the design of microcantilever waveguides [23] which will lead to lower cost and higher portability. The optical read-out method is also suitable for high throughput systems with a microarray format. A time

Manuscript received April 10, 2013; revised July 30, 2013; accepted September 30, 2013. Date of publication January 09, 2014; date of current version March 25, 2014. This paper was recommended by Associate Editor J. Chen.

Y. C. Lim, A. Z. Kouzani, and A. Kaynak are with the School of Engineering, Deakin University, Waurn Ponds, VIC 3216, Australia (e-mail: yangchoonlim@gmail.com; abbas.kouzani@deakin.edu.au; akif.kaynak@deakin.edu.au).

W. Duan is with the School of Medicine, Deakin University, Waurn Ponds, VIC 3216, Australia (e-mail: wei.duan@deakin.edu.au).

X. J. Dai is with the Institute for Frontier Materials, Deakin University, Waurn Ponds, VIC 3216, Australia (e-mail: jane.dai@deakin.edu.au).

D. Mair is with the Melbourne Centre for Nanofabrication, Clayton, VIC 3168, Australia (e-mail: douglas.mair@monash.edu).

Color versions of one or more of the figures in this paper are available online at http://ieeexplore.ieee.org.

Digital Object Identifier 10.1109/TBCAS.2013.2286255

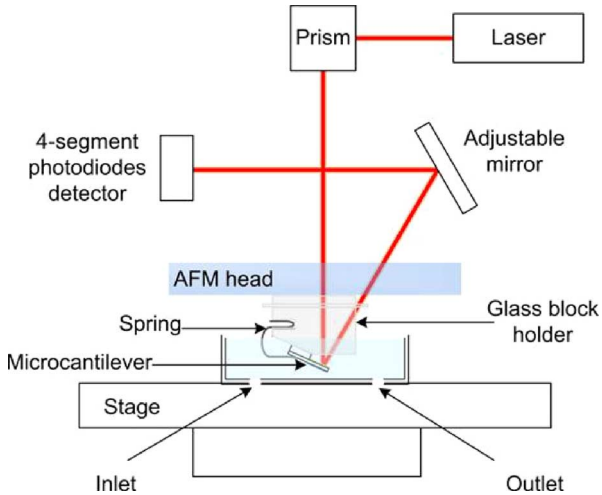

Fig. 1. Aptasensor measurement setup.

multiplexing scheme can be employed for measuring the displacement of the array of microcantilevers [24].

This paper presents the design and development of a microcantilever-based aptasensor employing SU-8 polymer as its fabrication material. To the best of our knowledge, this is the first study reported on the immobilisation of aptamers on bare SU-8 using gas plasma treatment. Surface modification using the plasma technique is more advantageous because it is a dry single step method, simple to implement, and has good reproducibility.

II. Aptasensor Design

The aptasensor design consists of a beam that is fixed at one end. The top side of the cantilever is immobilised with biorecognition elements for target sensing. The bottom side of the cantilever is coated with a layer of gold so that a laser beam could be deflected off its surface for beam deflection measurement via an optical read-out method during the biomolecules detection (Fig. 1). In this study, the displacement of the fabricated beam due to the detection of target analyte is validated using an atomic force microscope.

A modelling and simulation of the aptasensor was performed using the finite element method. *Coventorware*, a MEMS multiphysics software, was used to implement the modelling and simulation of the aptasensor. The beam model consists of three layers. The bulk layer is the SU-8 layer, which was coated with a thin monolayer to serve as the adsorbate layer. A thin layer of gold was deposited on the bottom side of the beam to serve as a reflective surface for the laser beam during optical lever detection.

Based on the literature, typical surface stress generated by the biomolecular interactions is 10 mJm^{-2} [25]. This value is used to simulate the surface stress in all the studies. The surface stress (σ_{s}) is the integral of the equivalent film stress (σ_{m}) in the monolayer over its thickness (t_{m}). It is represented by, $\sigma_{\mathrm{s}} = \int_0^{\mathrm{t_m}} \sigma_{\mathrm{m}} \mathrm{dz}$. The monolayer in this model was assumed to have 1 nm thickness. Therefore, to simulate the surface stress, a normal stress of 10 MPa was applied biaxially in the x and y-direction in the adsorbate layer. The simulated microcantilever beam models were meshed using the Manhattan parabolic mesh incorporating 500 elements. The effects of the microcantilever construction material and microcantilever geometries on the aptasensor sensitivity were investigated.

TABLE I
Material Properties of Different Simulated Materials

Properties	Polysilicon	Silica	Silicon nitride	SU-8
Young's modulus, E (GPa)	160	73	315	4.40
Poisson ratio, ν	0.22	0.17	0.27	0.22
Density, ρ (kgm^{-3})	2230	2200	3184	1190

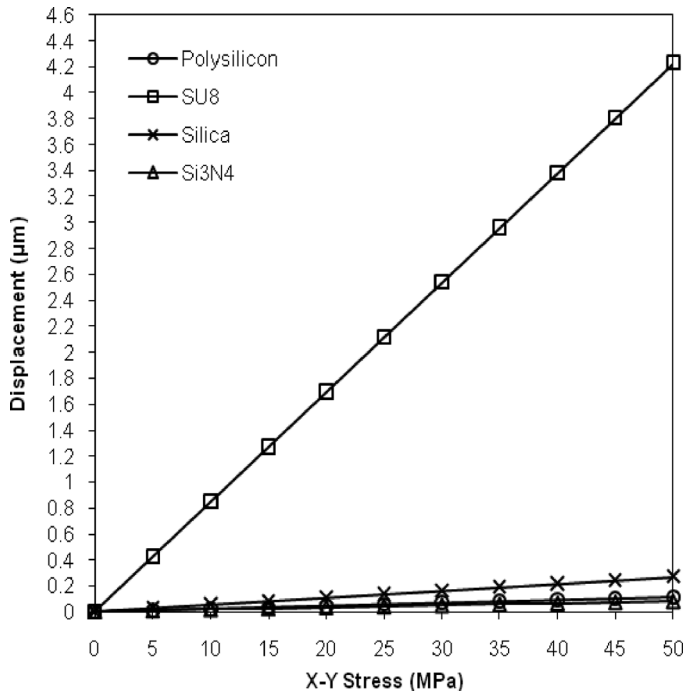

Fig. 2. Graph illustrating the displacement for various microcantilever materials.

A. Effect of Microcantilever Material

Polysilicon, silica, and silicon nitride are the common materials used in microcantilevers fabrication. However, a polymer such as SU-8 is a more attractive alternative due to its lower Young's modulus compared to the silicon counterparts (see Table I). The low Young's modulus means low stiffness which leads to more bending and subsequently larger displacement. The stiffness or spring constant, k, of the microcantilever beam is given by the formula, $k = \mathrm{Ewt}^3/4l^3$, where E, w, t and l are the Young's modulus, width,, thickness and length of the microcantilever, respectively. A microcantilever beam with the dimensions of 600 μm$\times$ 200 μm$\times$ 2 μm was implemented for the simulation studies. The simulated materials are homogenous, isotropic, and obey Hooke's law.

According to Fig. 2, the microcantilever made of SU-8 polymer would generate the highest displacement followed by that made of silica, polysilicon, and silicon nitride. Upon

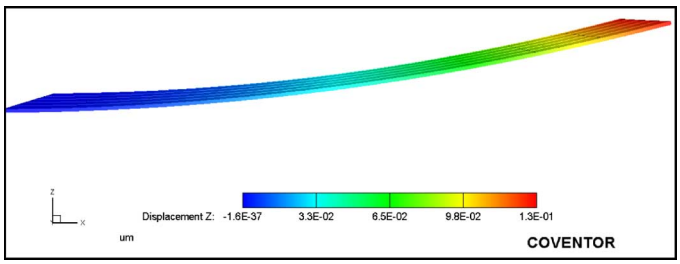

Fig. 3. Simulated beam displacement for 400 μm long beam.

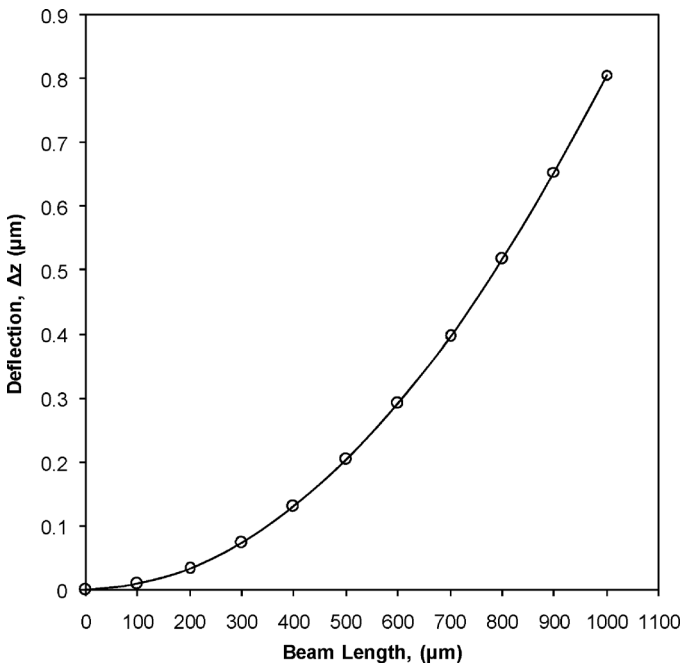

Fig. 4. Graph showing the relationship between the displacement and the length of the microcantilever.

target binding, the SU-8 microcantilever with the lowest spring constant would result in a more sensitive response than the materials with higher spring constants.

B. Effect of Microcantilever Geometries

To investigate the effect of geometrical dimensions of the microcantilever beam on the aptasensor sensitivity, FEM modelling and simulations were conducted for various conditions. The first simulation investigated the influence of the length of the cantilever beam on the microcantilever sensitivity. A SU-8 rectangular beam with a constant width of 50 μm and thickness of 2 μm and a varying length was modelled (Fig. 3). The effect of the thickness of the microcantilever beam on the sensor sensitivity was also investigated. In this study, the length and width of the beam were kept constant at 100 μm and 50 μm, while the thickness of the beam was varied using the parametric study function in *Coventorware*. The displacement of the beam for different beam thicknesses was observed.

Based on the simulation results presented in Figs. 4 and 5, larger beam displacements are generated when (i) the length of the beam is increased, and (ii) the thickness of the beam is decreased. Therefore, the displacement of the beam is proportional to l^2 but inversely proportional to t^2.

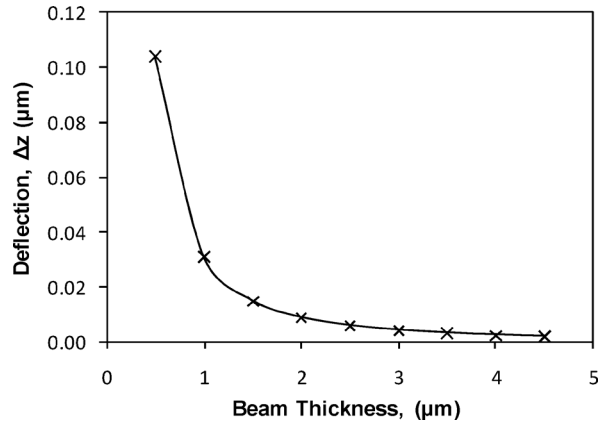

Fig. 5. Graph showing the displacement of the microcantilever beam for different thicknesses.

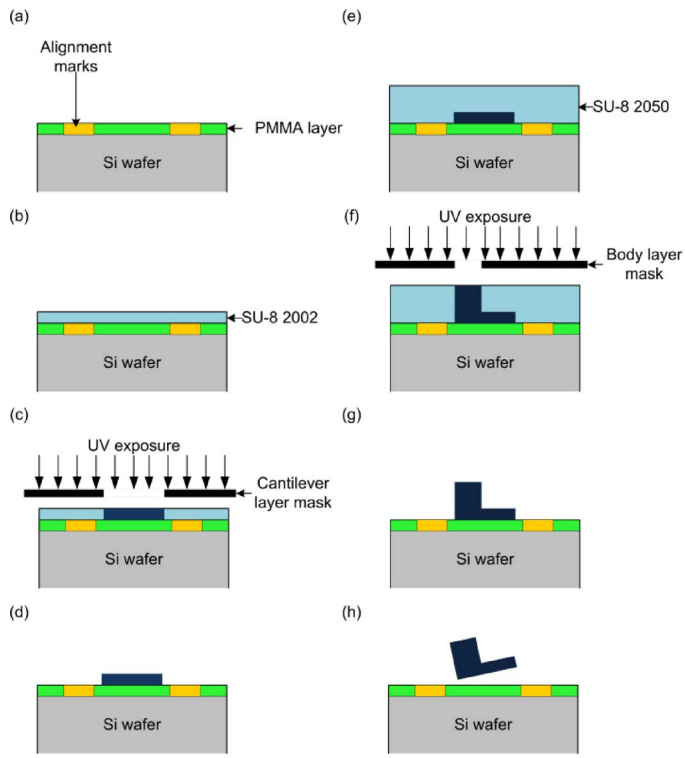

Fig. 6. Diagram illustrating the fabrication process. (a) Deposition of the sacrificial layer, followed by (b) spin coating of the microcantilever layer. (c) The SU-8 layer was exposed to UV after softbake to form the microcantilevers. (d) Removal of the non-cross-linked regions. (e) Thicker SU-8 photoresist was spun on top of the previous layer. After softbake, the SU-8 layer was exposed to UV to form the body layer. (g) Uncross-linked regions were developed. (h) Final structure was released from the substrate.

III. Aptasensor Fabrication

The microcantilever consists of two layers: a microcantilever layer for biomolecule sensing, and a body layer for device handling and transportation. The fabrication of the SU-8 microcantilever was achieved via the surface micromachining technique as shown in Fig. 6.

Firstly, the silicon substrate was cleaned using piranha solution to remove organic contaminants. Piranha solution was made by mixing equal parts of sulphuric acid 96% and hydrogen peroxide 30% in a beaker. The silicon wafer was

immersed in the piranha solution for 20 min, followed by a DI water rinse for 5 min. The rinsing step was repeated for three cycles, where fresh DI water used in each cycle. Alignment marks were patterned on the substrate using a lift-off technique to facilitate in features alignment during UV exposure for multilayer structure fabrication. Positive photoresist AZ4562 was used as the sacrificial material for the lift-off process.

Polymethylmethacrylate (PMMA), a positive photoresist, was spun onto the wafer to serve as a sacrificial layer. This enabled the release of the final structure from the silicon wafer at the end of the fabrication process. 5 ml of PMMA A6 was dispensed onto the wafer and spin coated at 500 rpm for 2 min at acceleration of 100 rpms^{-1}. Subsequently, the wafer was baked on hotplate at 170°C for 5 min. The resultant thickness was approximately 700 nm. After the curing of the sacrificial layer, 4 ml of SU-8 2002 was spun on top of PMMA to form the microcantilever layer. The spin coater was set to an acceleration of 100 rmps^{-1} and a spin speed of 500 rpm for 5 sec. Then, the acceleration was increased to 300 rpms^{-1} and a spin speed of 1500 rpm for 30 sec. Using a profilometer, the resulting thickness of the film was measured, and had an average of 2.16 μm.

A softbake was performed on a digital programmable hotplate ramping from room temperature to 65°C at 120°C hr^{-1} and held for 1 min. The temperature was further ramped up to 95°C at 120°C hr^{-1} and held for another minute. The wafer was left to cool to room temperature prior to UV exposure. The wafer was exposed with a constant dose of 80 mJcm^{-2}. A post exposure bake at 65°C was carried out for 1 min, and 95°C for another minute with the same ramping rate of 120°C hr^{-1}. After cooling the wafer to room temperature, the wafer was developed by immersing in SU-8 developer for a minute followed by an IPA rinsing to remove the non-cross-linked parts. The wafer was left to dry at ambient temperature as blow drying the wafer would lead to undesired deformation of the microcantilever on the wafer due to a strong pressure from the air gun in addition to the stress induced through rapid cooling due to the increased evaporation of IPA.

Then, 4 ml of SU-8 2050 was dispensed onto the wafer and the acceleration spin speed was set to 100 rpms^{-1} and spin speed of 500 rpm for 5 sec. This was then followed by increasing the acceleration speed to 300 rpms^{-1} and spin speed of 1500 rpm for 30 sec. The mean thickness of the microcantilever was 90 μm. Similar to SU-2002, a softbake step was performed directly after spin coating. The softbake parameters were 5 min at 65°C with a ramping rate of 120°C hr^{-1} from room temperature, followed by 21 min baking at 95°C at 120°C hr^{-1}.

The wafer was then exposed to UV with a constant dose of 240 mJcm^{-2}. Post exposure bake parameters were 1 min at 65°C with a ramping rate of 120°C hr^{-1} from room temperature and 11 min at 95°C at 120°C hr^{-1}. Finally, the substrate (Fig. 7) was soaked in SU-8 developer for 15 min, and another 15 min in fresh developer followed by a rinsing with IPA to remove the uncross-linked SU-8 for the body layers. A thin layer of gold was sputtered onto one side of the microcantilever surface to enable the laser beam to reflect off the microcantilever surface during the optical read-out.

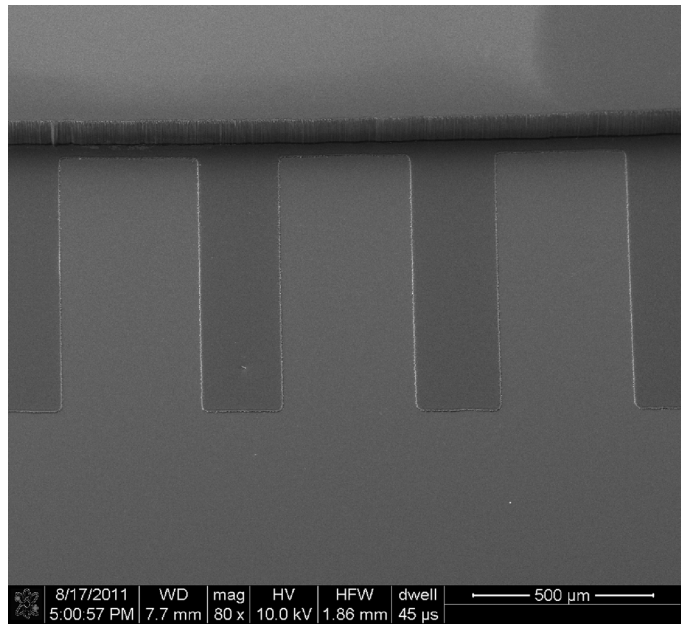

Fig. 7. SEM image of the fabricated microcantilever structure before releasing from the silicon substrate.

IV. Biological Evaluation

To demonstrate the proof-of-concept of the aptasensor, biological testings were conducted. Thrombin molecule was chosen as the system model. It is reported that thrombin plays a role in many diseases including thrombosis, neuronal diseases such as Alzheimer's [26], and pulmonary metastasis [27]. In addition, thrombin is a major target for anticoagulation and cardiovascular disease therapy [28]. Thrombin-aptamer binding has been vigorously investigated and characterised. As such, demonstrating thrombin detection using the developed aptasensor is very relevant for point-of-care diagnostics and drug discovery. Thrombin consists of several functional regions which include the active site, a polar binding site, and two anion-binding exosites; anion-binding exosite I or also referred to as fibrinogen-recognition exosite, and anion-binding exosite II or also referred to as heparin-binding exosite [29]. Immobilisation of bioreceptor molecules of target analyte is necessary in order to achieve high specificity in biosensors. Thrombin DNA aptamer (TBA15-1) was employed as the bioreceptor molecule. TBA15-1 aptamer primarily binds to the fibrinogen-recognition exosite of thrombin with dissociation constant, $\mathrm{K_d}$ of 100 nM [30].

A. Surface Immobilisation

During immobilisation, it is crucial to ensure that there is a good linkage between the biosensor substrate surface and the immobilised bioreceptor molecules so that they are not easily displaced by biological medium. It is also important to control the orientation of the bioreceptor molecules during surface immobilisation so that the active sites of the immobilised bioreceptor molecules face the biological medium, and are easily accessed by target analyte. It is essential that the immobilised receptor molecules maintain their biological activity while retaining their native 3D structure and good stability.

TABLE II
PLASMA CONDITIONS

Parameters	Argon	Continuous wave	Pulsed
Power, (W)	50	50	50
Pressure, (mbar)	0.05	0.05	0.05
Time, (s)	30	5	30
Duty cycle, (%)	-	-	5

According to the literature, so far no work has been published on aptamer immobilisation on SU-8 surface. In addition, most of the studies report on surface functionalisation using wet chemical methods. There is no investigation conducted on surface functionalisation using plasma for the immobilisation of aptamers. To the best of our knowledge, although there are reported works on plasma treated SU-8 for surface wettability modification [31], [32], the method presented in this paper is the first reported work on plasma SU-8 surface modification for aptamer immobilisation.

Plasma treatment of the SU-8 surface was conducted using an in-house built reactor inductively coupled with RF 13.56 MHz [33]. Plasma treatment was performed in a 30 cm-long and 7.5 cm-radius tubular glass reactor enclosed in a Faraday cage. A specially designed antenna in the inlet of the chamber acted as the plasma source, leaving the rest of the chamber as the afterglow area. It could transfer more than 100% of the RF power into the plasma using the incorporated RF matching network. Also, it could operate either in a continuous wave mode or a pulsed mode.

The microcantilever surfaces were cleaned before surface functionalization by dipping in piranha solution for 3 mins, followed by a rinsing in DI water for 5 mins. The rinsing step was repeated thrice. Then, the microcantilevers were placed in the plasma source area and the chamber was evacuated to achieve a base pressure lower than 1×10^{-3} mbar using a rotary pump.

Oxygen functional groups were introduced to the surface via oxygen gas plasma treatment. A combination of continuous plasma and pulsed plasma modes was used. Argon plasma was applied for surface cleaning and activation prior to oxygen plasma treatment. Then, continuous wave oxygen plasma was applied to the microcantilever surface followed by a pulsed oxygen plasma treatment. This combined plasma mode gave a uniform treatment with higher levels of the required functional groups [17], [34]. The plasma parameters are listed in Table II. After the plasma treatment, the gas flow was stopped and the aptasensor was left in the chamber under vacuum for 30 min to allow the surface to stabilise before exposing to air.

The oxygen functional groups on the surface had to be activated before immobilisation of aptamers. A total of 200 μl of 1:1 of 0.2 M of 1-[3-(dimethylamino)propyl]-3-ethylcarboiimide hydrochloride(EDC), and 0.05 M of N-hydroxysulfosuccinimide(sulfo-NHS) were mixed in sodium phosphate (PBS) buffer. Hydrochloric acid (HCl) was added to the activation solution to reduce the pH value to 6. The microcantilever was left soaking for 1 hr in a freshly prepared activation solution. Then the microcantilever was rinsed with DI water and pure ethanol, and left to dry at ambient temperature.

The activated surface was then immersed in solution of 0.1 M PBS buffer pH 7 containing 0.1 μM of 3'-end amine modified thrombin DNA aptamer for 2 hr at room temperature. The aptamers were heated at 85°C for 5 min, then allowed to cool to room temperature for 10 min, and subsequently incubated at 37°C for 15 min prior to immobilisation. This treatment facilitated the folding of aptamers so that the amine moiety at aptamer 3'-end was easily accessible for interaction with oxygen functional groups on the aptasensor surface. The surface was rinsed with 200 μl 1 mg/ml bovine serum albumin (BSA) solution in 0.1 M PBS buffer thrice for about 30 mins to remove physically adsorbed thrombin DNA aptamer and to block the remaining oxygen functional groups. The blocked aptamer surface was soaked in 0.1 M PBS buffer to remove unbound BSA for 10 min, and was rinsed thoroughly with PBS buffer. XPS analysis was performed to characterise the functional groups on the SU-8 surface before and after the oxygen plasma treatment. The XPS spectra were obtained using a K-Alpha X-ray photoelectron spectrometer from Thermo Fischer Scientific using monochromatic X-rays focused to a 400 μm spot size. Excessive charging of the samples was minimized using a flood gun; nevertheless, the C1s binding energies of SU-8 were accurately established by charge shift correcting the lowest binding energy peak of the C1s to 284.6 eV. Survey spectra were obtained at pass energy of 100 eV while high resolution peak scans were performed at 20 eV pass energy. The peak scans were employed to obtain the composition in terms of elemental C, O, N and Sb.

A Dimension® Icon® Atomic Force Microscope from Veeco Instruments Inc was used to characterise the surface roughness of the aptasensor before and after plasma treatment, as well as after aptamer immobilisation. Tapping mode was chosen instead of contact mode for surface scanning to prevent the microcantilever tip from dragging the biomolecules on the SU-8 surface. A contact angle tester was used to examine the wettability property of the SU-8 surface. DI water was utilised in the experiment. In addition, fluorescence microscopy using Fluoview® FV10i from Olympus was conducted to verify the successful immobilisation of aptamer on the plasma treated surface. Due to the small dimensions of the fabricated device, all surface characterisations were performed on a larger rectangular piece, which was simultaneously treated with the microcantilever sample.

B. Thrombin Detection

The microcantilever needed to be calibrated prior to biological testing in order to get accurate measurements. The microcantilever was calibrated and characterised using the JPK NanoWizard® II AFM. The fabricated SU-8 microcantilever was fixed to a glass block holder with a spring using a pair of tweezers, and mounted on the AFM head. A clean glass slide was placed at the sample holder situated on the AFM stage. The microcantilever was moved towards the glass slide surface using the JPK auto approach. A force-distance curve was obtained and the linear portion of the curve was used for sensitivity fitting within the calibration manager. After obtaining the sensitivity measurement, the spring constant of the microcantilever was obtained using a thermal noise measurement technique. The microcantilever was retracted from the

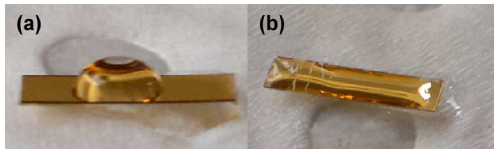

Fig. 8. (a) Water contact angle of pristine SU-8 surface. (b) Water contact angle of oxygen plasma treated SU-8 surface.

glass slide surface, and the deflections of the microcantilever induced by thermal fluctuations were measured. The frequency and magnitude of these fluctuations were obtained and fitted with Lorentz curve to calculate the spring constant value. The obtained spring constant value was 1.389 mN/m.

For the detection of thrombin molecules, the optical level read-out method was implemented. The fabricated microcantilevers were mounted onto the NanoWizard® II AFM using a pair of tweezers by clamping the microcantilevers to a glass block holder via a spring and attaching it to the AFM head. The deflection of the microcantilever was determined by reflecting a laser beam off the gold-coated surface of the microcantilever. A four-segment photodiode was used to detect the angle of deflection. A BioCell™ coverslip based fluidic cell (from JPK Instruments AG, Berlin, Germany) with a volume capacity of 400 μl was mounted onto the AFM stage for thrombin detection in a controlled environment. The detection system setup is depicted in Fig. 1.

The thrombin molecules solution obtained from a supplier was aliquot and diluted to the desired concentration before use. Prior to introducing the thrombin molecules into the fluidic cell, the microcantilevers were equilibrated in the buffer solution for an hour (0.1 M Tris-acetate pH7.4) to obtain a baseline of the deflection of the microcantilevers.

1 μM of thrombin in binding buffer solution was injected to the fluidic cell and incubated for 30 min. Next, the buffer solution was introduced to remove unbound thrombin molecules on the microcantilever surface. The deflection of the microcantilever was monitored in-situ using the real-time oscilloscope function in the SPM software developed by JPK. The measurements were recorded in a static environment without the continuous flow of the buffer solution. The binding experiment was conducted in a controlled temperature of $27 \pm 0.2°\mathrm{C}$. A microcantilever with immobilised control aptamers served as a control sample in the experiment to test nonspecific interactions.

V. Results and Discussions

A. Surface Morphology

Pristine SU-8 surface is highly hydrophobic. Fig. 8 shows the surface wettability of the SU-8 surface. When a droplet of water was dropped onto the surface of the untreated SU-8, the measured contact angle was 89.4° [Fig. 8(a)]. After oxygen plasma treatment, the surface property of SU-8 changed from hydrophobic to hydrophilic with a measured contact angle of 10.3° [Fig. 8(b)].

Fig. 9(a) shows the morphology of a 1 $\mu\mathrm{m} \times 1$ $\mu\mathrm{m}$ surface area of SU-8 before plasma treatment. The surface was quite smooth with an RMS roughness of 3.44 nm. After oxygen plasma treatment, the RMS roughness increased to 17.95 nm [Fig. 9(b)]. This shows that the oxygen plasma treatment caused the surface corrugation which was not observed in the pristine SU-8 surface. It was also observed that a uniform nanostructured surface had been formed at the plasma treated sample.

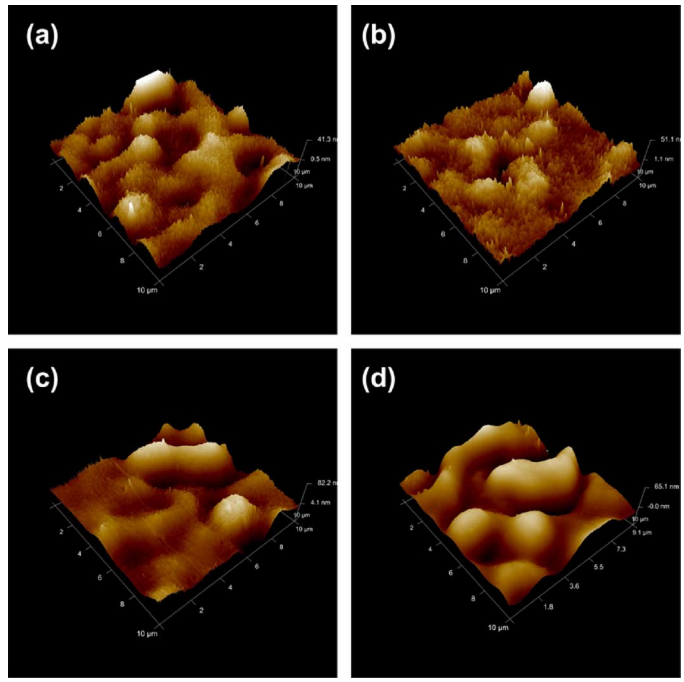

Fig. 9. Morphology of (a) pristine SU-8 surface, (b) oxygen plasma treated SU-8 surface, (c) thrombin DNA aptamer immobilised on plasma treated SU-8 surface, and (d) SU-8 surface after thrombin binding.

After aptamer immobilisation, the surface RMS roughness of plasma treated surface reduced to 11.68 nm [Fig. 9(c)]. This is because the aptamer molecules are larger in size compared to the functional groups grafted on the SU-8 surface. Thrombin molecules had successfully bound to the immobilised aptamers on the aptasensor surface. After thrombin-aptamer binding [Fig. 9(d)], the surface morphology showed that the surface had become flatter and smoother with an RMS roughness value of 7.23 nm.

B. XPS Analysis

The main composition of the SU-8 surface includes carbon, oxygen, nitrogen and antimony (Table III). The presence of nitrogen on the surface could be due to surface contamination. The untreated SU-8 shows a higher percentage of carbon compared to the oxygen plasma treated SU-8. The oxygen plasma treatment increased the oxygen concentration by 10.21%. These results demonstrate that oxygen has been incorporated on the SU-8 microcantilever surface.

Functional groups on the SU-8 surface were characterised via analysis of high resolution XPS C1s peaks. The C1s spectra for untreated SU-8 surface [Fig. 10(a)] consists of three peaks at binding energy of 284.6 eV (C-C/C-H) , 286.3 eV (C-O), and288.5 eV ($\mathrm{O-C=O}$) After plasma treatment [Fig. 10(b)], the peak at 284.6 eV was reduced by 15.6% from 59.31% to 43.71%. Meanwhile, the peak at 288.5 eV reduced by 7.08%

TABLE III
ELEMENTAL COMPOSITION OF PRISTINE AND O_2 TREATED SU-8 SURFACE

	Pristine SU-8	O_2 plasma treated SU-8
Carbon, %	76.54	69.19
Oxygen, %	15.82	26.03
Nitrogen, %	5.98	2.05
Antimony, %	1.66	2.73

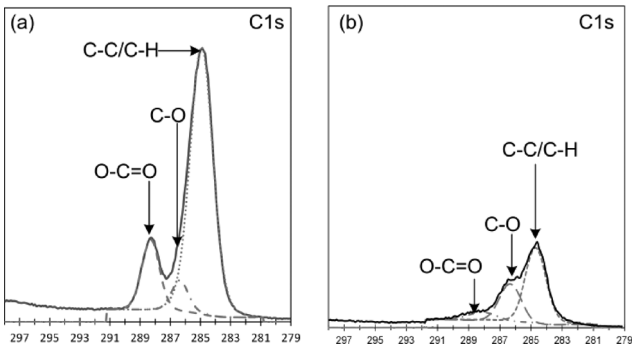

Fig. 10. XPS analysis for (a) pristine SU-8 surface and (b) oxygen plasma treated SU-8 surface.

from 12.05% to 4.97%. An increase from 5.18% to 20.52% was observed at the peak of 286.3 eV, showing an improvement of 15.34%. This indicated that the hydroxyl functional groups increased while the C-C and $\mathrm{O-C=O}$ decreased considerably after the plasma treatment.

The oxygen plasma treatment cleaved the residual epoxide groups on the surface and introduced hydroxyl functional groups. This resulted in the change of surface wettability in SU-8 from hydrophobic to hydrophilic. The oxygen functional groups bind the aptamers to the sensor surface via electrostatic interactions and hydrogen bonding with the amine functional groups in the aptamers.

C. Fluorescence Microscopy

To verify the successful immobilisation of aptamers and subsequent binding of the thrombin molecules, fluorescence microscopy was carried out using FITC-tagged thrombin molecules. The experiment was conducted on 3 samples which include a control sample with aptamers immobilised on pristine SU-8 surface, oxygen treated SU-8 surface, and a negative control with aptamers exposed to FITC-tagged human Factor Xa. Human Factor Xa is smaller than thrombin molecule (MW: 46 kDa) and does not bind to TBA-15. The negative control was employed to access the non-specific binding background. Fluorescence signal intensity was observed after exposing the surface to FITC-tagged thrombin molecules and after washing/rinsing of the surface with buffer solution. It was observed that the fluorescence signal intensity on pristine SU-8 surface was reduced significantly indicating that most of the biomolecules were washed away.

Fig. 11 shows the fluorescence signal detected on the microcantilever sensor surface when the surface of the sensor was exposed to FITC-tagged thrombin. Patches of weak fluorescence signal are shown in Fig. 11(a). Meanwhile, the plasma treated SU-8 produced the highest fluorescence signal showing that thrombin molecules have successfully bound to the aptamers

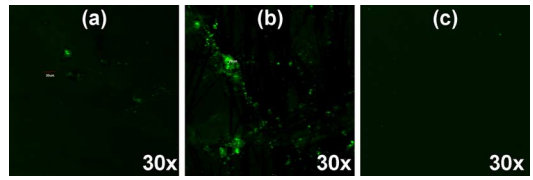

Fig. 11. Fluorescence microscopy images showing the binding of FITC-tagged thrombin molecules with aptamers immobilised on the sensor surface. (a) Pristine SU-8 surface. (b) Oxygen plasma treated SU-8 surface. (c) Negative control employing FITC-tagged Factor Xa as the binding molecule.

immobilised on the plasma treated SU-8 surface [Fig. 11(b)]. This demonstrates that the plasma treated SU-8 surface provides a strong and stable anchorage surface for the aptamers. For the negative control [Fig. 11(c)], it was observed that there was non-detectable fluorescence signal indicating that there was no non-specific binding on the sensor surface. This shows that the aptamer immobilised on the sensor surface binds specifically to thrombin molecules.

D. Characterisation and Biological Evaluation

In the optical lever read-out, a photodetector measures the differential voltage between the four segments of the photodiodes when determining the microcantilever deflection. To obtain the microcantilever displacement z, the measured deflection in volts, z_v is converted using a conversion factor known as sensitivity, S, whereby $z = Sz_v$.

Sensitivity of the microcantilever is related to the constant slope in the repulsive region of the obtained force-distance curve. The equation describing this relationship can be written as $S = \Delta z_p/\Delta z_v$. The measured sensitivity value was $1.378\,\mu\mathrm{mV}^{-1}$.

The spring constant of the fabricated microcantilever was calculated using a fitting algorithm by applying the equipartition theorem to the area under the resonance peak. The measured spring constant was $1.389\ \mathrm{mNm}^{-1}$ while the theoretical calculation was $1.604\ \mathrm{mNm}^{-1}$, producing a percentage error of 13.39%. The theoretical calculation was based on the formula, $k = Ewt^3/4l^3$. The fabricated microcantilever spring constant was one order of magnitude lower than that of the silicon nitride microcantilever and is consistent with that reported literature [16].

To improve the interaction and binding accessibility between thrombin DNA aptamers and thrombin molecules, the detection of thrombin molecules was conducted in binding buffer solution (Tris-acetate pH7.4). This favoured the aptamer to fold into a G-quadruplex structure, a 3D structure configuration with intricate binding pockets that binds specifically to the thrombin binding domain.

SU-8 polymer experiences drift in liquid environment. The drift observed in SU-8 polymer is about $0.3\ \mathrm{nm\ s}^{-1}$ higher than that reported for silicon microcantilevers ($500\,\mu\mathrm{m} \times 100\,\mu\mathrm{m} \times 1\,\mu\mathrm{m}$) $5\ \mathrm{nm\ h}^{-1}$ [35]. This may be caused by absorption of liquid in the polymer [36]. To reduce the false positive signals, a differential displacement measurement was performed using a reference microcantilever. This eliminates the background noise caused by non-specific binding and sensor drift. Temperature in the fluidic cell was

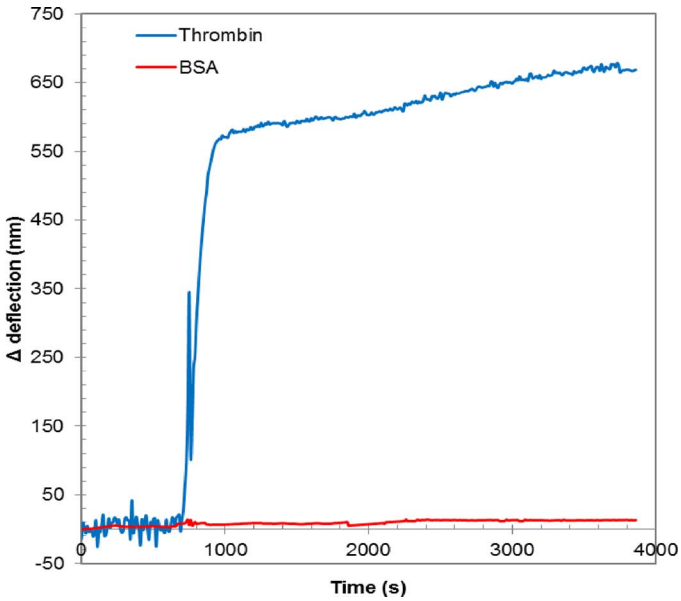

Fig. 12. Injection of 1 μM thrombin molecules in Tris-acetate buffer at pH 7.4. Graph shows the differential bending response of the aptasensor as a function of time.

kept constant to minimise thermal drift due to the bilayer beam construction. Measurement of the beam displacement was performed after a constant baseline was achieved in the buffer solution.

When 1 μM of thrombin was injected into the fluidic cell, the response curves, depicted in Fig. 12, shows an increase in the vertical differential deflection towards the positive direction with a maximum differential displacement of 590 nm. This corresponds to a sensitivity of 132.9 $\mu\mathrm{m}(\mathrm{Nm}^{-1})^{-1}$. In this work, the positive deflection value indicates that the aptasensor experienced compressive surface stress as the microcantilever with the immobilised surface was mounted inverted on the AFM head. On the other hand, a negative deflection magnitude indicates tensile surface stress. The displacement of the microcantilever beam was due to the change in differential surface stress between the immobilised layer and the blocked layer on the microcantilever surface generated during thrombin-aptamer binding. The obtained beam deflection value for the SU-8 aptasensor was of one order of magnitude higher than that made of silicon nitride. This means that the fabricated aptasensor was able to generate a larger displacement for the same amount of surface stress which leads to a higher aptasensor sensitivity.

To evaluate the specificity of the aptasensor, BSA was injected and incubated for the same amount of time, 30 min in the binding buffer solution. It can be seen from the red line in Fig. 12 that the aptasensor did not produce any measurable deflections. This demonstrates that the aptasensor binds specifically to thrombin molecules.

VI. Conclusions

The paper presented the design, development, and surface immobilisation of a surface-stress-based microcantilever aptasensor using SU-8, which is a negative photoresist epoxy-acrylate polymer, highly transparent in the UV region, biocompatible, chemically resistant and has a low Young's modulus. A novel plasma treatment technique that utilised a combination of continuous wave plasma and pulsed plasma modes was used to produce a uniform treatment with higher functional groups on the aptasensor surface for aptamer immobilisation. Surface morphology and fluorescence microscopy results show that the aptamer immobilisation was successful using the developed protocols. The proof-of-concept demonstration of the aptasensor was carried out using thrombin molecules, and the response curve was successfully obtained. The fabricated aptasensor demonstrates high specificity, showing insignificant response when microcantilever surface was exposed to negative control BSA molecules.

The stability of the SU-8 microcantilever biosensor for variations in pH and temperature is crucial, and not much work has been conducted to investigate it. Calleja *et al.* [37] compared the effect of pH, temperature and ionic strengths on SU-8 microcantilevers, and compared them to gold-coated silicon cantilevers. It was found that fluorocarbon-coated SU-8 microcantilever reduced thermal drift in the system compared to thiol-coated silicon nitride. Our future work will focus on the stability of SU-8 microcantilever in liquid environment.

We expect that the cost of the mass produced version of the device would be lower than that of the microcantilever biosensors constructed from different materials. This is due to the fact that the use of SU-8 enables a simpler, cheaper, faster, and more flexible fabrication process. In addition, aptamers are highly regarded as an emerging class of receptor molecules offering cost-effectiveness that can further lower the production cost of a biosensor. These factors make the aptasensor cheaper than conventional biosensors, e.g., silicon-based microcantilever biosensors, when mass produced.

Acknowledgment

The authors would like to thank Mr. Z. Chen for his help with plasma equipment training, Ms. J. Lin for her advice and assistance in biological evaluation experiments, Dr. S. Shigdar for her help in confocal microscope training, Dr. K. Magniez for technical discussions, and Ms. G. D. Rajmohan and RMIT University for their assistance with XPS analysis. This work was performed in part at the Melbourne Centre for Nanofabrication (MCN) in the Victorian Node of the Australian National Fabrication Facility (ANFF).

References

[1] S. D. Jayasena, "Aptamers: An emerging class of molecules that rival antibodies in diagnostics," *Clin. Chem.*, vol. 45, pp. 1628–1650, Sep. 1999.

[2] S. M. Nimjee, C. P. Rusconi, and B. A. Sullenger, "Aptamers: An emerging class of therapeutics," *Annu. Rev. Med.*, vol. 56, pp. 555–583, 2004.

[3] Y. C. Lim, A. Z. Kouzani, and W. Duan, "Aptasensors: A review," *J. Biomed. Nanotechnol.*, vol. 6, pp. 93–105, 2010.

[4] H. Ozaki, A. Nishihira, M. Wakabayashi, M. Kuwahara, and H. Sawai, "Biomolecular sensor based on fluorescence-labeled aptamer," *Bioorg. Med. Chem. Lett.*, vol. 16, pp. 4381–4384, 2006.

[5] B. Li and Z. Zhang, "Chemiluminescence flow biosensor for determination of total D-amino acid in serum with immobilized reagents," *Sens. Actuators B, Chem.*, vol. 69, pp. 70–74, 2000.

[6] E. Mariani, M. C. G. Monaco, S. Sgobbi, J. F. de Zwart, A. R. Mariani, and A. Facchini, "Standardization of a micro-cytotoxicity assay for human natural killer cell lytic activity," *J. Immun. Methods*, vol. 172, pp. 173–178, 1994.

[7] X. D. Zhu, "Comparison of two optical techniques for label-free detection of biomolecular microarrays on solids," *Opt. Commun.*, vol. 259, pp. 751–753, 2006.
[8] X. Yan, Y. Lvov, H.-F. Ji, A. Singh, and T. Thundat, "A general microcantilever surface modification method using a multilayer for biospecific recognition," *Org. Biomol. Chem.*, vol. 1, pp. 460–462, 2003.
[9] B. Li, Y. Du, H. Wei, and S. Dong, "Reusable, label-free electrochemical aptasensor for sensitive detection of small molecules," *Chem. Commun.*, pp. 3780–3782, 2007.
[10] W. Shi-Wei and M. S. C. Lu, "Cmos capacitive sensors with sub *U*m microelectrodes for biosensing applications," *IEEE Sensors J.*, vol. 10, pp. 991–996, 2010.
[11] K. Jee-Yeon, A. Jae-Hyuk, C. Sung-Jin, I. Maesoon, K. Sungho, J. P. Duarte, K. Chang-Hoon, P. T. Jung, L. S. Yup, and C. Yang-Kyu, "An underlap channel-embedded field-effect transistor for biosensor application in watery and dry environment," *IEEE Trans. Nanotechnol.*, vol. 11, pp. 390–394, 2012.
[12] M. Curreli, Z. Rui, F. N. Ishikawa, C. Hsiao-Kang, R. J. Cote, Z. Chongwu, and M. E. Thompson, "Real-time, label-free detection of biological entities using nanowire-based fets," *IEEE Trans. Nanotechnol.*, vol. 7, pp. 651–667, 2008.
[13] R. Raiteri, M. Grattarola, H.-J. Butt, and P. Skládal, "Micromechanical cantilever-based biosensors," *Sens. Actuators B, Chem.*, vol. 79, pp. 115–126, 2001.
[14] M. Yue, J. C. Stachowiak, H. Lin, R. Datar, R. Cote, and A. Majumdar, "Label-free protein recognition two-dimensional array using nanomechanical sensors," *Nano Lett.*, vol. 8, pp. 520–524, 2008.
[15] R. Marie, H. Jensenius, J. Thaysen, C. B. Christensen, and A. Boisen, "Adsorption kinetics and mechanical properties of thiol-modified DNA-oligos on gold investigated by microcantilever sensors," *Ultramicroscopy*, vol. 91, pp. 29–36, 2002.
[16] M. Calleja, M. Nordström, M. Álvarez, J. Tamayo, L. M. Lechuga, and A. Boisen, "Highly sensitive polymer-based cantilever-sensors for DNA detection," *Ultramicroscopy*, vol. 105, pp. 215–222, 2005.
[17] Z. Chen, X. J. Dai, P. R. Lamb, D. R. de Celis Leal, B. L. Fox, Y. Chen, J. du Plessis, M. Field, and X. Wang, "Practical amine functionalization of multi-walled carbon nanotubes for effective interfacial bonding," *Plasma Process. Polymers*, vol. 9, no. 7, pp. 733–741, Jul. 2012.
[18] C. L. Britton, R. L. Jones, P. I. Oden, Z. Hu, R. J. Warmack, S. F. Smith, W. L. Bryan, and J. M. Rochelle, "Multiple-input microcantilever sensors," *Ultramicroscopy*, vol. 82, pp. 17–21, 2000.
[19] G. Shekhawat, S.-H. Tark, and V. P. Dravid, "MOSFET-embedded microcantilevers for measuring deflection in biomolecular sensors," *Science*, vol. 311, pp. 1592–1595, Mar. 2006.
[20] W. Shu, S. Laurenson, T. P. J. Knowles, P. K. Ferrigno, and A. A. Seshia, "Highly specific label-free protein detection from lysed cells using internally referenced microcantilever sensors," *Biosens. Bioelectron.*, vol. 24, pp. 233–237, 2008.
[21] L. A. Pinnaduwage, V. I. Boiadjiev, J. E. Hawk, A. C. Gehl, G. W. Fernando, and L. C. R. Wijewardhana, "An energy conservation approach to adsorbate-induced surface stress and the extraction of binding energy using nanomechanics," *Nanotechnol.*, vol. 19, p. 105501, 2008.
[22] M. Nordström, S. Keller, M. Lillemose, A. Johansson, S. r. Dohn, D. Haefliger, G. Blagoi, M. Havsteen-Jakobsen, and A. Boisen, "SU-8 cantilevers for bio/chemical sensing; fabrication, characterisation and development of novel read-out methods," *Sensors*, vol. 8, pp. 1595–1612, 2008.
[23] S. T. Koev, R. Fernandes, W. E. Bentley, and R. Ghodssi, "A Cantilever sensor with an integrated optical readout for detection of enzymatically produced homocysteine," *IEEE Trans. Biomed. Circuits Syst.*, vol. 3, no. 6, pp. 415–423, 2009.
[24] H. P. Lang, M. K. Baller, R. Berger, C. Gerber, J. K. Gimzewski, F. M. Battiston, P. Fornaro, J. P. Ramseyer, E. Meyer, and H. J. Güntherodt, "An artificial nose based on a micromechanical cantilever array," *Analytica Chimica Acta*, vol. 393, pp. 59–65, 1999.
[25] S. Satyanarayana, D. T. McCormick, and A. Majumdar, "Parylene micro membrane capacitive sensor array for chemical and biological sensing," *Sens. Actuators B, Chem.*, vol. 115, pp. 494–502, 2006.
[26] F. M. Donovan, C. J. Pike, C. W. Cotman, and D. D. Cunningham, "Thrombin induces apoptosis in cultured neurons and astrocytes via a pathway requiring tyrosine kinase and RhoA activities," *J. Neurosci.*, vol. 17, pp. 5316–5326, Jul. 1997.
[27] M. L. Nierodzik and S. Karpatkin, "Thrombin induces tumor growth, metastasis, and angiogenesis: Evidence for a thrombin-regulated dormant tumor phenotype," *Cancer Cell*, vol. 10, pp. 355–362, 2006.
[28] V. Schroeder, T. Chatterjee, H. Mehta, S. Windecker, T. Pham, N. Devantay, B. Meier, and H. P. Kohler, "Thrombin Activatable Fibrinolysis Inhibitor (TAFI) levels in patients with coronary artery disease investigated by angiography," *Thrombos. Haemostas.*, vol. 88, pp. 1020–1025, 2002.
[29] W. Bode, "Structure and interaction modes of thrombin," *Blood Cells, Molecules, Diseases*, vol. 36, pp. 122–130, 2006.
[30] L. C. Bock, L. C. Griffin, J. A. Latham, E. H. Vermaas, and J. J. Toole, "Selection of single-stranded DNA molecules that bind and inhibit human thrombin," *Nature*, vol. 355, pp. 564–566, 1992.
[31] W. Ferdinand, P. Davidovskaya, S. Zürcher, M. Kaiser, H. Herberg, A. Gigler, and R. W. Stark, "Stability of the hydrophilic behavior of oxygen plasma activated SU-8," *J. Micromech. Microeng.*, vol. 17, p. 524, 2007.
[32] F. Walther, T. Drobek, A. M. Gigler, M. Hennemeyer, M. Kaiser, H. Herberg, T. Shimitsu, G. E. Morfill, and R. W. Stark, "Surface hydrophilization of SU-8 by plasma and wet chemical processes," *Surf. Interface Anal.*, vol. 42, pp. 1735–1744, 2010.
[33] R. Landgraf, M. K. Kaiser, J. Posseckardt, B. Adolphi, and W. J. Fischer, "Functionalization of polymer sensor surfaces by oxygen plasma treatment," *Procedia Chem.*, vol. 1, pp. 1015–1018, 2009.
[34] L. Li, X. J. Dai *, H. S. Xu, J. H. Zhao, P. Yang, G. Maurdev, J. d. Plessis, P. R. Lamb, B. L. Fox, and W. P. Michalski, "Combined continuous wave and pulsed plasma modes: For more stable interfaces with higher functionality on metal and semiconductor surfaces," *Plasma Process. Polymers*, vol. 6, pp. 615–619, 2009.
[35] M. K. Baller, H. P. Lang, J. Fritz, C. Gerber, J. K. Gimzewski, U. Drechsler, H. Rothuizen, M. Despont, P. Vettiger, F. M. Battiston, J. P. Ramseyer, P. Fornaro, E. Meyer, and H. J. Güntherodt, "A cantilever array-based artificial nose," *Ultramicroscopy*, vol. 82, pp. 1–9, 2000.
[36] M. Tenje, S. Keller, S. Dohn, Z. J. Davis, and A. Boisen, "Drift study of Su8 cantilevers in liquid and gaseous environments," *Ultramicroscopy*, vol. 110, pp. 596–598, 2010.
[37] M. Calleja, J. Tamayo, M. Nordstrom, and A. Boisen, "Low-noise polymeric nanomechanical biosensors," *Appl. Phys. Lett.*, vol. 88, pp. 113901–113901-3, 2006.

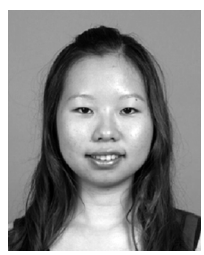

Yang Choon Lim received the B.Eng. degree (first class honors) in robotics and the Ph.D. degree from Deakin University, Waurn Ponds, Australia, in 2006 and 2012, respectively.

She was a Research Fellow in the School of Engineering, Deakin University. Currently, she is an Instrument Manager at the Melbourne Centre for Nanofabrication, Clayton, Australia. Her research interests include biological-micro-electro-mechanical systems for clinical diagnostics.

Abbas Z. Kouzani (M'95) received the M.Eng. degree in electrical and electronics engineering from the University of Adelaide, Adelaide, Australia, and the Ph.D. degree in electrical and electronics engineering from Flinders University, Bedford Park, Australia, in 1995 and 1999, respectively.

He was a Lecturer in the School of Engineering, Deakin University, Waurn Ponds, Australia, and then a Senior Lecturer with the School of Electrical Engineering and Computer Science, University of Newcastle, Callaghan, Australia. Currently, he is an Associate Professor in the School of Engineering at Deakin University. He has been involved in over $2 million research grants including Australian national competitive, industry, and university grants. He has authored over 220 refereed papers. He has carried out applied research and consultancy for several companies. His research interests include various aspects of BioMEMS. Currently, he is supervising seven Ph.D. candidates.

Dr. Kouzani is an OzReader with the Australian Research Council and reviews for a number of international journals and conferences. He is the leader of the Deakin University's BioMEMS Research Group.

Wei Duan graduated from a medical school in Shanghai, China, and received the Ph.D. degree from the University of Melbourne, Parkville, Australia, in 1991.

He taught medicine and engaged in the research into molecular cell biology and novel therapeutics of cancer at the National University of Singapore. He is currently with Deakin Medical School, Waurn Ponds, Australia, where he heads a nanomedicine program to develop cancer-targeting aptamers and nanoparticles for cancer molecular imaging and targeted drug delivery.

Xiujuan J. Dai received B.Sc. and M.Sc. degrees in plasma physics and semiconductor physics, respectively, from universities in China, and the Ph.D. degree in plasma physics from the Australian National University, Acton, Australia, in 1996.

Her research has focused on the development of novel plasma technologies and methodologies; the development of materials with new functionality for energy and biomedical applications using semiconductors, metals, ceramics, polymers, and textiles; and improved understanding of the underlying mechanisms through various surface characterizations, analysis, and diagnostics. She has been internationally recognized for her contributions to plasma science and technology. She established a new plasma laboratory at IFM since joining Deakin University, Waurn Ponds, Australia, in 2009. She has grown many collaborations across the university and outside research organizations, nationally and internationally. Currently, she is supervising 10 Ph.D. candidates.

Dr. Dai was an invited speaker at the Gordon Research Conference (USA) on plasma science and technology in 2000, and joint recipient of the CSIRO Research Medal and a NanoVic Prize in 2006 for her work on carbon nanotubes.

Akif Kaynak received the B.Sc. degree from the University of Manchester, Manchester ,U.K., the M.Sc. degree from Rutgers University, New Brunswick, NJ, USA, and the Ph.D. degree from the University of Technology, Sydney (UTS), Australia.

After receiving the Ph.D. degree in 1994, he was employed as an Assistant Professor in the Department of Engineering Sciences, Middle East Technical University (METU), Ankara, Turkey, then as a Research Fellow at the Queensland University of Technology (QUT), Kelvin Grove, Australia, before joining the School of Engineering, Deakin University, Waurn Ponds, Australia, in 2001. Currently, he is an Associate Professor in mechanical engineering. Subjects he teaches include physics, statics, dynamics, stress analysis, fibre science, and materials science. His research interests are polymer coatings, functional textiles, and sensors. He is a regular reviewer for various international journals and a coinventor in a patent on conducting polymer coated wool.

Douglas Mair graduated with a degree in electrical and electronic engineering from Caledonian University, Glasgow, Scotland, in 1993.

He was an Instrument Manager at the Melbourne Centre for Nanofabrication, Clayton, Australia, looking after photolithography, atomic layer deposition, and furnace processes. He has worked in industry for the majority of his career, mainly with Motorola's semiconductor division as a Failure Analysis Engineer.